引用格式：CHEN Zhuo, LI Tiancheng, SUN Degui, et al. Digital Thermo-optic Switch of SOI Waveguide Based on Goos-Hänchen Spatial Shift of Reflected Mode[J]. Acta Photonica Sinica, 2021, 50(4):0423001
陈卓,李天成,孙德贵,等. SOI波导反射模式的古斯-汉欣空间位移效应及其数字式热光开关[J].光子学报,2021,50(4):0423001

SOI波导反射模式的古斯-汉欣空间位移效应及其数字式热光开关

陈卓[1],李天成[2],孙德贵[1],孙娜[1],尚鸿鹏[1],陈晨[1]
(1 长春理工大学 理学院,长春 130022)
(2 长春长光圆辰微电子技术有限公司,长春 130022)

摘 要:借助波导转角镜结构,利用古斯-汉欣空间位移和热光效应折射率调制的有效组合,提出了波导反射模式数字式热光开关结构。在给定入射角的条件下优化了空间古斯-汉欣位移,在具有古斯-汉欣效应的本征态下,反射光束出现了较大的跳跃。在1.0 μm厚硅膜的绝缘体上硅平台上,单模输入波导和多模干涉波导结构之间的导模本征态匹配,验证了1×3数字式光开关功能。实验中,器件结构引起的光损耗为0.3 dB,开关功率为130~150 mW,开关时间约为50 μs,相邻输出端之间隔离度为15 dB。与马赫-曾德尔干涉仪型的2×2热光开关和等离子体效应热光开关的最新结果进行比较证明了该数字式热光开关的先进性。

关键词:数字式光开关;热光效应;古斯-汉欣效应;SOI波导
中图分类号: **文献标识码**:A **doi**:10.3788/gzxb20215004.0423001

Digital Thermo-optic Switch of SOI Waveguide Based on Goos-Hänchen Spatial Shift of Reflected Mode

CHEN Zhuo[1], LI Tiancheng[2], SUN Degui[1], SUN Na[1], SHANG Hongpeng[1], CHEN Chen[1]
(1 *School of Science, Changchun University of Science and Technology, Changchun* 130022, *China*)
(2 *Changchun Changguang Yuanchen Microelectronics Technology Co. Ltd, Changchun* 130022, *China*)

Abstract: With the waveguide corner mirror structure and the effective combination of the Goos-Hanchen (GH) spatial shift and the thermo-optical effect refractive index modulation, a digital thermo-optical switch structure of waveguide reflected mode is proposed. The GH spatial shift is optimized under the condition of a given incident angle, and the reflected beam has a larger jump under an eigenstate with the GH effect. On a silicon-on-insulator platform with a 1.0 μm thick silicon film, the guided mode eigenstate matching between the single-mode input waveguide and the multimode interference waveguide structure verifies the function of a 1×3 digital optical switch. In experiment, the optical loss caused by the device structure is 0.3 dB, the switching power is 130~150 mW, the switching time is about 50 μs, and the isolation between adjacent output ports is 15 dB. The comparison with the latest results of the Mach-

Foundation item: Human Resources and Social Security Talent Plan Fund of Jilin Province (No. 634190874002), Natural Science Foundation of Jilin Province (No. 20180101223JC)
First author: CHEN Zhuo (1995—), male, M.S. degree candidate, mainly focuses on silicon-based optical waveguide device. Email: mrchen9506@163.com
Corresponding author: SUN Degui (1960—), male, professor, Ph. D. degree, mainly focuses on integrated photonics device technology. Email: sundg@cust.edu.cn
Received: Nov.16, 2020; **Accepted**: Dec.24, 2020

Zehnder interferometer 2×2 thermo-optic switch and the newly emerging plasma effect thermo-optic switch shows the advancement of this digital TO switch.

Key words: Digital optical switch; Thermo-optic effect; Goos-Hänchen effect; SOI waveguide
OCIS Codes: 230.7370; 230.7390; 230.2090

0 Introduction

With the increase of bandwidth and capacity of optical communication networks, the new regimes and technologies of communication components and modules continue to emerge. Based on Planar Light-wave Circuit (PLC) and Photonic Integrated Circuit (PIC) on silicon wafers, the optical functional components such as optical splitter, Wavelength Division Multiplexing (WDM) device, Optical Switch (OS), etc. are all playing the key roles[1]. In traditional optical communications systems, as a typical analog optical switch, Mach-Zehnder Interferometer (MZI) configuration has widely been deployed to implement highly integrated optical switches and switch matrices[2-4]. As presented below, in the MZI-type optical switch, a half-wave optical phase modulation is required to implement one switching operation and the output values are dependent of the modulated physical parameter. Silicon-On-Insulator (SOI) platform has presented its exclusive merits in developing high-performance functional components, both the Thermo-Optic (TO)[5-9] and the Electro-Optic (EO) switches have been attracting intensive interests[10-13]. In research and development of the applications of SOI optical switches, the large-scale optical switching systems need the Digital Optical Switch (DOS) since it is insensitive to a deviation of the modulating signal, resulting in the stable switching operations.

At the beginning of this century, a lot of regimes of waveguide couplers were proposed for the applications of DOS systems. The typical establishments are based on adiabatic couplers, including the $LiNbO_3$ waveguide adiabatic coupler based on EO DOS by KRAHENBUHL R et al. in 2002[14], the EO DOSs using polymeric waveguide adiabatic couplers by YUAN W in 2005[15], and the adiabatic MMI coupler having digital operations by SOLEHMAINEN K et al[16], and in 2005 we realized digital TO switch using polymer waveguide in previous work[17], and a large-scale silicon photonic matrix switch with a vertical coupler was studied by SEOK T J et al[18]. Since the silicon film of SOI-platform was reported to have the semiconductor Free-Carrier Dispersion (FCD) effect, the high-bandwidth nanoscale waveguide EO switches have been extensively studied. An excellent work in DOS was reported in 2009 by CAMPENHOUT J V et al. using the asymmetric cascaded regime of MZI structures[4]. In 2013, we first theoretically demonstrated the quantum Goos-Hänchen (GH) spatial shift, and then proposed a possible regime of digital optical switches and further in 2016 both quantum states of the spatial and angular GH shifts were theoretically demonstrated for the DOS functions[19-20].

For the dielectric waveguide based TO switches, the plasmonic heating effect of electric field at the interface of dielectric and metal materials has also exhibited a potential in applications due to its big phase transition under a sub-volt voltage. In such a device, the broadband hybrid plasmonic-vanadium dioxide switch, and then the silicon MOS micro-nano structure is a very significant upgradation of the plasmonic-effect TO switches with CMOS technique[20-21]. Therefore, a P-channel MOS structure of field-effect transistor (PMOSFET) was first exploited to implement a silicon optoelectronic micro-nano scaled structure.

In this work, on the SOI waveguide platform, a DOS is demonstrated with the GH spatial shift in which the numerical simulations based on the theoretical model for the device performance is validated by both the software simulations and the experimental results.

1 Device concepts and theoretical investigation

1.1 Device concepts and theoretical models

As well known, when an optical beam travels from medium 1 to medium 2, with the refractive indices n_1 and n_2, respectively, and $n_1 > n_2$, an optical Total Internal Reflection (TIR) happens at the interface of these two media. Figure 1 shows the schematic relationship of incident and reflected beams, where the incident angle is θ. In an optical TIR process, a common physical phenomenon is the GH effect, which can cause both the spatial and angular shifts. The GH spatial shift Δ is defined to be the effective spatial shift of the reflected beam at the direction perpendicular to the propagating direction of the reflected beam with respect to the ideal position

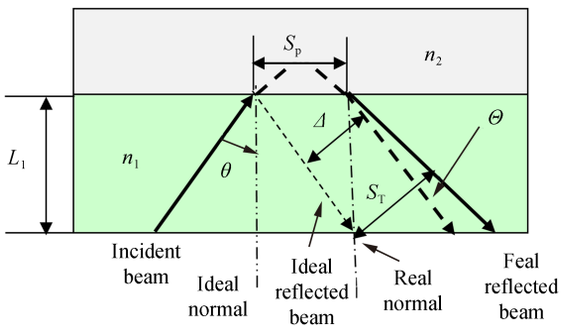

Fig. 1 Schematic relationship of the incident

and the GH angular shift Θ is defined to be the effective angular change of the reflected beam with respect to the ideal reflection direction. The displacement at the reflective interface is defined as S_p.

Research shows that the phase change of reflected beam is a key parameter in the GH spatial shift, and its change with incident angle is theoretically demonstrated to be a quantum photonic process, which is controlled by the delay time of the photon beam tunneling process in penetration depth[19]. Thus, as the scientists of the United States performed and predicted, it is reasonable for the reflected beam to display a small angular deviation from the law of specular reflection in the time of 1985/86[22-23]. Until two decades later, in 2006 and 2009, the experimental results of the angular shift under the GH effect were observed in microwave and optical domains, respectively[24-25]. In the optical experiments, the general role of GH spatial and angular shifts is modeled with both the phase and amplitude of reflected beam, then the total beam displacement is defined by a linear combination of the spatial shift Δ and angular shift Θ as [19, 25].

From the reflection coefficient $r = R \cdot \exp(i\phi)$, the algebra expression of the GH shift can be expressed as

$$D = \frac{\partial \ln r}{\partial \theta} = \frac{1}{R}\frac{\partial R}{\partial \theta} + i\frac{\partial \varphi}{\partial \theta} \tag{1}$$

Then, if λ is the wavelength of optical beam, the propagation constant of input guided-mode is defined as $k_{in} = 2\pi n_1 / \lambda$, then the spatial and angular shifts in the GH effect as[19, 25]

$$\Delta = \frac{1}{k_{in}}\frac{\partial \varphi}{\partial \theta} = \mathrm{Im}(\ln r) \tag{2}$$

$$\Theta = -\frac{2}{(k_{in}^2 \cdot w_o^2)}\frac{1}{R}\frac{\partial R}{\partial \theta} = \mathrm{Re}(\ln r) \tag{3}$$

where w_o stands for the waist of an approximated Gaussian beam of reflected guided-mode. Therefore, in terms of the set of Eqs. (2) and (3), both the GH spatial and angular shifts have involved with both the amplitude and phase of the whole reflected beam. As shown in Fig.1, the thickness of medium 1 is set to be L_1 so that a single mode beam can be maintained from the reflective interface to the output edge, then the total spatial shift from the ideal reflected beam is determined by both the spatial and angular shifts as[20]

$$S_T = (\Delta + L_1 \cdot \Theta)/\cos\theta \tag{4}$$

It can be noticed from Eqs. (2) and (3) that the spatial shift is related with phase of the reflected wave, while the angular shift has a relation with both the amplitude and phase of the reflected wave. Then, a 1×3 TO DOS regime is proposed based on a combination of the GH shift and the TO phase modulation as depicted in Fig.2. This DOS is composed of one single-mode input waveguide and three single-mode output waveguides, an SOI Waveguide Corner Mirror (WCM) structure and a Multi-mode (M-mode) structure that is designed to have a length of L_1. Among three output ports, the middle one is labeled as Out 0, the left and the right ones are, respectively, labeled as Out −N and Out +N. When a light beam is launched into the input waveguide that has an incident angle larger than critical angle of TIR, the coefficient amplitude and phase of the reflected wave as R and ϕ, respectively. A TIR with a GH shift happens to the reflected beam, and finally the optical beam is designed to get out at the port Out 0. Then, when a TO Refractive Index Modulation (RIM) is applied to the interface area, the TIR condition will be changed and the GH shift will have a plus or a minus change to switch the output beam from Out 0 to Out +N or Out −N. Since the GH shift change was ever proved to be a quantum process, this switching operation is a digital optical switch function.

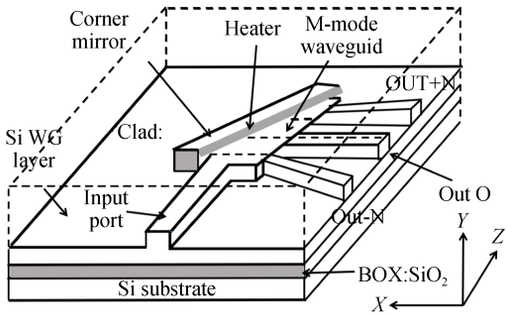

Fig. 2 Schematic construction of the SOI waveguide corner structure and GH effect based 1×3 optical switch with microscale waveguides and TO-RIM

1.2 Numerical simulations for GH shifts

In terms of the feasible fabrication condition for this project on the SOI platform, the WCM based TO DOS are designed as: the thickness of SOI substrate is 525 μm, the thicknesses of both the SiO_2 BOX layer and silicon film are 1.0 μm, the top cladding layer is a 1.0 μm thick SiO_2 film, the rib width and height are optimized to be 4.0 μm and 0.5 μm, respectively. By setting the refractive indices of the SiO_2 BOX layer of the silicon film as 1.444 and 3.43, with FDTD calculation we obtain the effective indices of 3.325 4 and 3.316 8 for TE and TM modes, respectively, then for the mirror material of Si_3N_4 with a refractive index of 2.00, the critical angles of the Total Internal Reflection (TIR) are 37.0° and 37.1° for TE and TM modes, respectively, so in the following simulations, an incident angle range of 36～45° to selected to cover these two critical angles. At the wavelength λ=1 550 nm, with Eqs. (1)～(4) and our self-edited Matlab programs, we obtain the dependences of the GH spatial and angular shifts on the incident angle for both TE and TM modes as shown in Figs.3(a) and 3(b), respectively. In these two figures, the left and right vertical axes stand for the spatial and angular shifts, respectively, and + sign of the spatial shift indicates the shift of the reflected mode to the opposite side of the input beam and − sign of the spatial shift indicates the shift of the reflected mode to the same side of the input mode.

Note from Figs.3(a) and 3(b) that if the incident angle is greater than the two critical angles, only the spatial shift exists for both the TE-mode and TM-mode, which are about 5.0～1.0 μm and 2.5～1.0 μm, respectively, while the angular shift is 0 for the two modes. The reason for such a small angular shift is very complicated. The simulation results for the tradeoff between transfer efficiency and the GH shift of the WCM structure leads the incident angle to the vicinity of 45°. At the incident angle of 45°, the initial GH spatial shift is ～1.0 μm for both TE- and TM-mode. In contrast, at the smallest incident angle of 38°, the initial GH spatial shift for TE-mode is ～5.0 μm, while that for TM-mode is only ～2.0 μm.

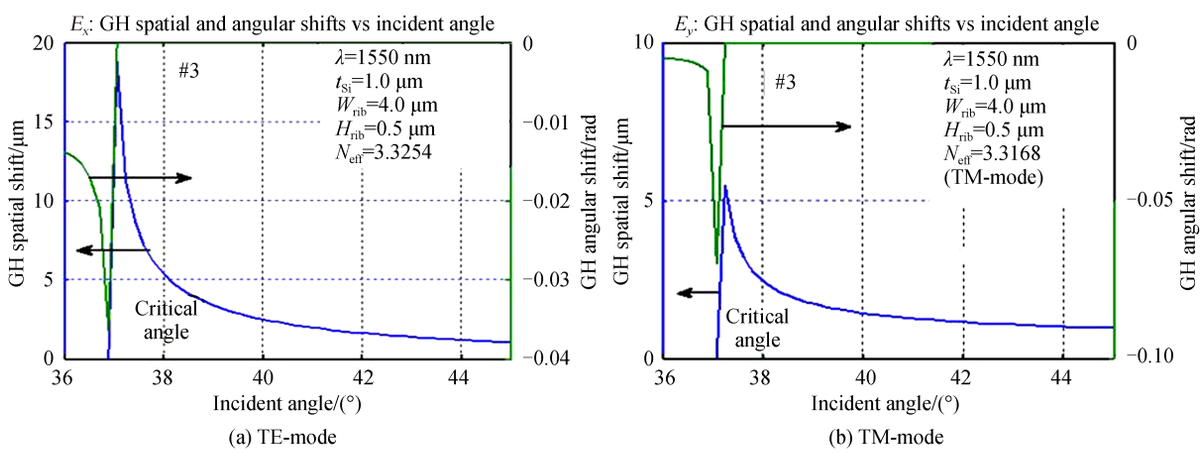

Fig. 3 Numerical simulations for the incident angle dependences of the GH spatial and angular shifts of a WCM structure

1.3 Finite difference time domain simulations for device optical performance

The simulations show obtained with Finite Difference Time Domain (FDTD) software that the device shown in Fig.3 can work for TE-mode rather than TM-mode, when the rib waveguide has the construction as that the buried SiO_2 film (BOX layer) has a 2.0 μm thickness and the silicon film has a 1.5 μm, the rib has a 4.0 μm width and a 0.5 μm height. Then, the single-mode waveguide is obtained and its power distributions at horizontal (x) and vertical (y) directions are shown in Figs.4(a) and 4(b), respectively. Note that the power distributions at both the horizontal and vertical directions are close to the expectable situation. According to the simulations shown in Figs. 3 and 4, in the design of a real device, only TE-mode performance will be investigated in the research below. In terms of the maintaining length of an M-mode structure for a single-mode input signal, we set L_1=400 μm, then the simulation results in Fig.3(a) show that around incident angle of 45°, the spatial GH shift change is about 1.0 μm. We know, the FDTD is the precision expansion of Maxwell′s equation for the travelling behavior of a guided mode because it considers all three space dimensions and one time-dimension - the finite difference in time domain.

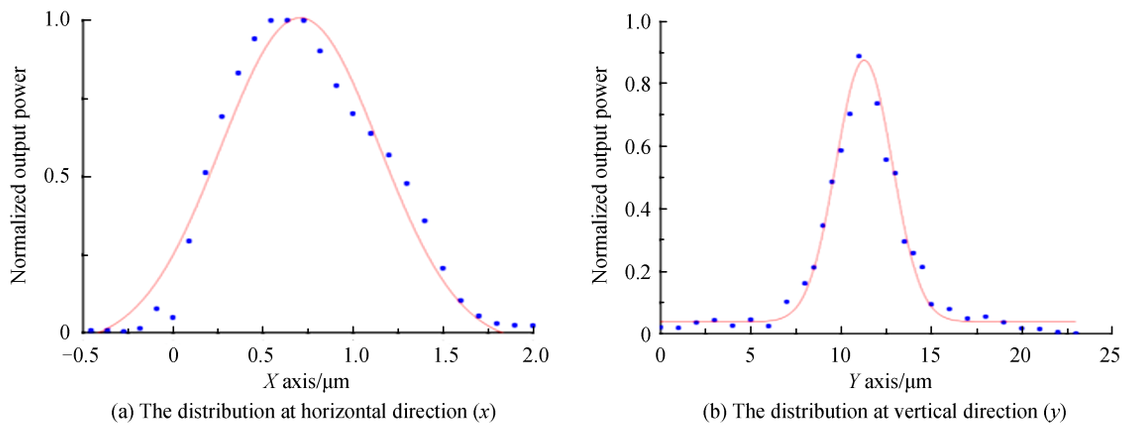

Fig.4 Simulation results of power distributions of a single-mode SOI rib waveguide

So, for a sharp turning waveguide structure, the FDTD algorithm is one of most powerful methods in processing the Maxwell′s equation. Thus, we designed a 1×3 switch configuration, as shown in Fig.5(a), then the FDTD simulation of its optical transfer efficiency is depicted in Fig.5(b), respectively, in which the initial GH shift as 1.0, 0 and −1.0 μm for the upper, the middle and the lower output waveguides, respectively. The output angles of the upper, the middle and the lower ports are designed to be (45°−1.0°), 45° and (45°+1.0°), respectively. With a single-mode waveguide with the rib width of 4.0 μm and the rib height of 0.5 μm, we obtain the accurate simulation results of optical outputs at the three output ports with the FDTD software as listed in Table 1. Note that the optical on-chip losses at the upper, the middle and the lower ports are P_1=−4.02, P_2=−21.74 and P_3=−28.54 dB, respectively. Thus, it turns out that the most of output power is at the upper output port that has an initial GH spatial shift of 1.0 μm, which is agreeable with the numerical

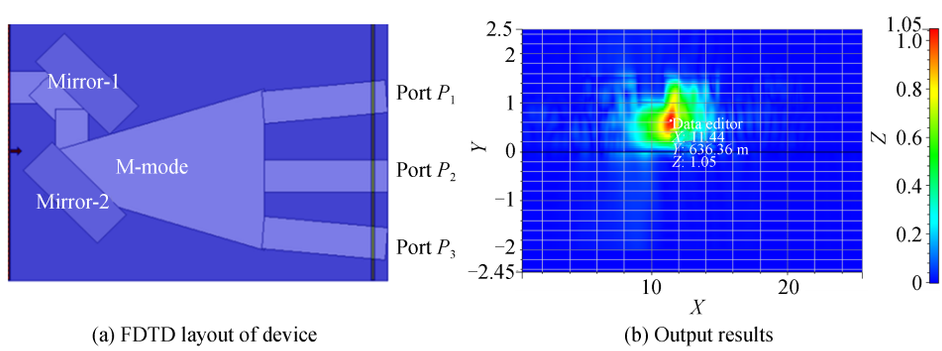

Fig.5 FDTD simulation of the GH spatial shift 1×3 optical switch with SOI microscale waveguide corner mirror and TO refractive index modulation

simulation results shown in Fig.3(a), and the initial isolation between the upper port from the adjacent port, the

Table 1 FDTD simulation results of the SOI-PIC 1×3 thermo-optic switch at OFF-state

Item	Outputs at three ports		
Number	Upper	Middle	Lower
Value /dB	−4.02	−21.74	−28.02

middle one, is about (−21.74−(−4.02)) =−17.72 dB. Similarly, we obtain the initial isolation between the lower port from the middle one, is about (−28.02−(−21.74)) =−6.28 dB. Thus, between P_1 and P_2 there is a high isolation as two output ports of a switch, while between P_2 and P_3 there is a low isolation. FDTD simulations show that the isolation between two adjacent outputs is dependent on the distance between these two ports.

2 Experiments and discussion

2.1 Design and fabrication of the experimental samples

As shown in Fig.6(a) we designed the real device samples with two WCM structures so that the optical performance can be measured with ease. The device dimensions are as W_r=4.0 μm, the M-mode structure is designed to be Multimode Interference (MMI) structure with W_{mmi}(input)=10.0 μm, W_{mmi}(output)=20.0 μm, and the connective waveguide between the two corners is the rib waveguide having a length of 30.0 μm. Then, the device samples were fabricated on an SOI substrate with a procedure as 1) etching silicon film for the rib waveguide layer; 2) etching silicon film to form the deep trenches at the corner mirror places; 3) depositing SiO_2 top layer to form both the mirrors and the top cladding layer; 4) depositing and etching the metal film to form the heaters. Totally, we designed and fabricated six experimental device samples of such a 1×3 TO DOS on one chip packaged on one PCB, in which the six devices having the same device structure as shown in Fig. 6 (a), in which a heating power is applied onto the second WCM to manipulate the switching operations of an incident optical beam. Figure 6(b) only shows the photo image of a fabricated device.

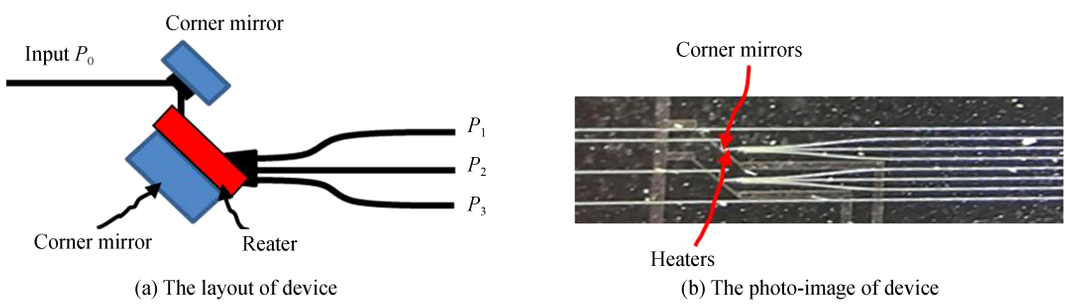

Fig.6 Device sample image of 1×3 digital TO switch based on an SOI WCM structure

2.2 Experiments and analysis

In experiments, a laser beam with the wavelength of 1 550 nm was launched into the input waveguide of switch through a standard single-mode fiber (SMF-28), the DC electrical power supply and a power meter were used for measuring the Insertion Losses (IL) and the isolation among the output ports, a function generator, a photodiode and an oscilloscope were used for measuring the switching speed. With a TE-mode input optical signal, the optical output images of a 1×3 optical switch sample at three ports are taken by a CCD camera as shown in Fig.7(a) where the output spots from the upper, the middle and the lower ports correspond with P_1, P_2 and P_3, respectively. Then, we measured the two-WCM-caused Optical Loss (OL) of five 1×3 optical switches at the three output ports as shown in Fig.7(b). The net two-WCM-caused OL of each 1×3 optical switch is obtained by subtracting the Insertion Loss (IL) of a straight waveguide from the IL of the switch device. Note that the expected output port at the unmodulated state (the upper port, Port1) has an average value of −0.3 dB for the five switch samples that is the net optical loss caused by the structure of two WCMs, while the output ports at the unmodulated state (the middle and lower ports, Port2 and Port3) have

the average OL values of −15.5 dB and −31.5 dB, respectively, so there is an isolation of 16 dB between any two adjacent outputs, which are basically consistent with the FDTD simulation values depicted in Table 1. Note that all the output powers at the three ports have the uniform optical loss specifications among the five devices. Further, the dynamic switching process of an input optical signal was carried out and the output results at the upper port (P_1) are shown in Fig.7(c) where the driving electrical signal has a frequency of 10 kHz, then the two switching times, the rise and fall times were measured to be 50 and 65 μs, respectively. The switching power was measured to be 150~200 mW, obviously it is higher than the one an SOI TO switch should have. Else note from Fig. 7(c) that the optical output response to the driving signal is very sharp, implying the quantum process existing in this switching operation. A direct reason for such a high switching power is that the fabricated switch configuration has not reached the optimal eigenstate of quantum GH spatial shift at the incident angle. As an indirect reason, due to the tradeoff between the optical transfer efficiency of the WCM structure and the fabrication condition, the GH angular shift has not been exploited yet. Accordingly, the advancements of digital TO switching functions could not be reached with the current configuration. It can be noticed that Fig.7(c) has shown an accurate response to the sharp process of the drive signal, which also presents the digital switching effect.

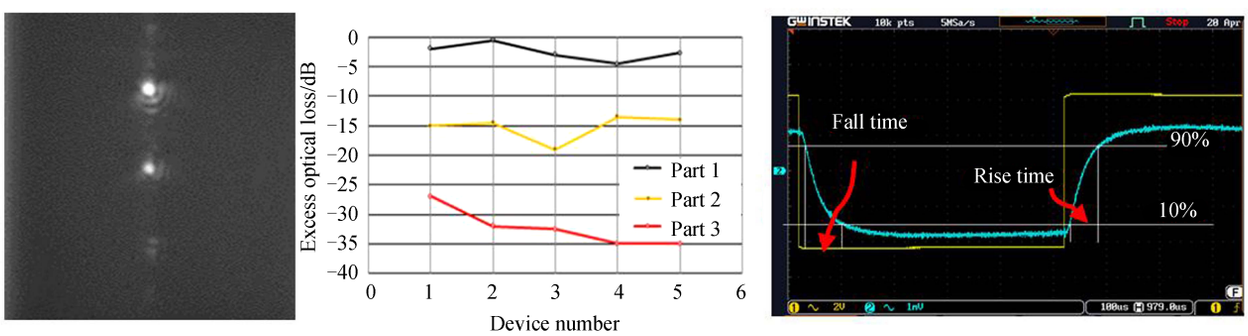

(a) Three output guided-modes (b) Tested optical on-chip losses (c) Measurements of switching speeds

Fig. 7 Performance measurements 1×3 optical switch

3 Comparison with the other type TO switch

As discussed in the introduction, the SOI waveguide based TO switches have experienced the extensive research and development for more than two decades. Despite many device configurations of SOI-waveguide TO switches are ever proposed and investigated, for the broadband applications, the MZI-type configurations are always at the dominant positions. In fact, the MZI-type optical switches include two constructions of beam splitter/combiner: the 3dB Directional Couplers (DCs) and the MMI couplers, but an SOI-waveguide MZI-type 2×2 TO switch must have an optical modulated phase of $\Delta\varphi = (2\pi/\lambda)\cdot(\Delta n L_H)$ between the two arms to realize one switching operation irrespective of the DC-type or MMI-type 3 dB couplers used, implying the analog switching functions[4-8,26]. Of course, the MMI coupler based MZI type 2×2 optical switches can significantly overcome the drawback in the output isolation using an adiabatic structure[5-6]. In contrast with the MZI type optical switch, for a TE-mode optical signal, the output of WCM TO switch, the total displacement of a reflected guide-mode at the end of the MMI structure defined by Eq. (1) meets the spatial separation of two output ports. If the refractive index of silicon material is not dispersive, the output power is in principle independent of wavelength.

In switching principle, the WCM-type TO switch, as discussed above, the output of a guided-mode is determined by only the total GH displacement which can be optimized in the aspects of the incident angle, the reflective angle, the MMI structure and the separation between two adjacent ports. In the footprint size, for the SOI-waveguides having the 1~2 μm thick silicon film and the 2~3 μm waveguide width, in an MZI switch, the corresponding coupling length of DC or MMI 3dB Couplers is in the range of 500~1 000 μm, while the heater length is generally over 500 μm to meet the optical phase modulation of π, then the final footprint length of a switch unit is generally over 1.0~2.0 mm. In contrast, for a WCM-type TO switch, the total length of one

unit can be $<$1.0 mm, and even can be reduced to 100～200 μm. Else, for the MZI type switches, the error of the coupling ratio δk_{dc} would become difficult to be controlled in fabrication irrespective of the DC or MMI type 3 dB couplers used, resulting in a deterioration of the output isolation of switch. To the contrary, the WCM-based optical switch configuration does not need to reach a fixed value of optical phase, instead needs to create a GH shift jump from one output port to the other. Meanwhile, the refractive index modulation meets the eigen conditions of effective index and position of the output guided mode, so the switching power and time can also be improved in several aspects, including the incident angle, the WCM structure and the heater structure, etc. Hence, the potentials of switching power and switching time are not predictable.

In fact, apart from the MZI and WCM type TO switches, some other new TO switch regimes were also studied, so the special designs and techniques have ever exploited to further improve the device performance in switching power and time. For instance, in 2005 CHU T, et al. published an MZI-based 1×4 TO switch with a 90 mW switching power and 100 μs switching time; and in 2010 SHOJI Y, et al published an ultrahigh extinction ratio 2×2 TO switch with a 60 mW switching power and 100 μs switching time[8,26]. The impressive achievements are: 1) the 2×2 SOI-waveguide TO switch using SOI folded-waveguide for the MZI structure with a 6.5 mW switching power and 14 μs switching time published by DENSMORE A et al. in 2009, and 2) the 2×2 SOI-waveguide TO switch using SOI free-standing strip waveguides with a 0.54 mW switching power and 140 μs switching time published by SUN P et al. in 2010[27-28]. In summary, for the SOI waveguide TO switches, the switching powers and times are 30～200 mW and 5～100 μs, respectively, so the measured results of switching power and time for the WCM-based TO switch sample studied in this paper are still in the reasonable ranges. In addition, as mentioned in Introduction, the plasmonic phase transition of electric-filed at a dielectric-metal interface has been attracting more attentions to implement micro-nano scale TO switches under the sub-volt electric field[29-31]. As the transparent optical switches of silicon photonic and optoelectronic integrated circuits[10-13], the other type semiconductor based opaque optical switch, is attracting more attention due to their excellent compatibility with CMOS technology.

4 Conclusion

As a conclusion, based on the quantum output selections of switching operations, the DOS regime in this work still has a large room to be improved in the device performance. For instance, the isolation between the two adjacent output ports, the switching time and the switching power can be improved much with the further optimization of the device architecture albeit the measured values of device performance are not impressive in this article. The agreement between the theoretical calculation, the FDTD simulation and the experimental results enhances the extension of the WCM based DOS on the SOI platform. The comparison with the other SOI-waveguide TO switches has apparently presented the advancements in optical performance despite the device configuration studied in this work has not been optimized. Thus, as a switching unit, it will have the substantial applications in the undergoing large-scale matrix TO switches.

References

[1] ORCUTT J S, MOSS B, SUN C, et al. Open foundry platform for high-performance electronic-photonic integration [J]. Optics Express, 2012, 20(11): 12222-12232.

[2] EARNSHAW M P, SOOLE, CAPPUZZO M, et al. 8 × 8 optical switch matrix using generalized Mach-Zehnder interferometers [J]. IEEE Photonics Technology Letters, 2003,15(6):810-812.

[3] ZHA Y, SUN D G, LIU T G, et al. Rearrangeable nonblocking 8 × 8 matrix optical switch based on silica waveguide and extended banyan network [J]. IEEE Photonics Technology Letters, 2007, 19:390-392.

[4] CAMPENHOUT J V, GREEN W M J, VLASOV Y A. Design of a digital, ultra-broadband electro-optic switch for reconfigurable optical networks-on-chip [J]. Optics Express, 2009, 17(26): 23793.

[5] SUN D G, HU Z, ABDUL-MAJID S, et al. Limitation factor analysis for silicon-on-insulator waveguide Mach - Zehnder interference-based electro-optic switch [J]. Journal of Lightwave Technology, 2011, 29(17): 2592-600.

[6] WATTS M R, SUN J, DEROSE C, et al. Adiabatic thermo-optic Mach-Zehnder switch [J]. Optics Letters, 2013, 38(5): 733-735.

[7] ZHAO Y, JIA H, XIA Y, et al. Reconfigurable nonblocking 5-port silicon thermo-optic optical router based on Mach-Zehnder optical switches [C]. ACPC. 2015. AS4A.5.

[8] SHOJI Y, KINTAKA K, SUDA S, et al. Low-crosstalk 2 × 2 thermo-optic switch with silicon wire waveguides [J].

Optics Express, 2010, 18(9): 9071-9075.
[9] RYAN A, ALEX F, CHRISTOPHER D, et al. Wideband silicon-photonic thermo-optic switch in a wavelength-division multiplexed ring network [J]. Optics Express, 2014, 22(7): 8205-8218.
[10] XING J, LI Z, ZHOU P, et al. Nonblocking 4×4 silicon electro-optic switch matrix with push-pull drive [J]. Optics Letters, 2013, 38(19): 3926-3929.
[11] KEN T, KEIJIRO S, MUNEHIRO T, et al. Ultra-compact 32 × 32 strictly-non-blocking Si-wire optical switch with fan-out LGA interposer [J]. Optics Express, 2015, 23(13):17599-17606.
[12] LU L, ZHAO S, ZHOU L, et al. 16 × 16 non-blocking silicon optical switch based on electro-optic Mach-Zehnder interferometers [J]. Optics Express, 2016, 24(9): 9295-307.
[13] NIKOLOVA D, CALHOUN D M, LIU Y, et al. Modular architecture for fully non-blocking silicon photonic switch fabric [J]. Microsystems & Nanoengineering, 2017, 3:16071.
[14] KRAHENBUHL R, HOWERTON M M, DUBINGER J, et al. Performance and modeling of advanced Ti: $LiNbO_3$ digital optical switches [J]. Journal of Lightwave Technology, 2002, 20(1): 92-99.
[15] YUAN W, KIM S, STEIER W H, et al. Electrooptic polymeric digital optical switches (DOSs) with adiabatic couplers [J]. IEEE Photonics Technology Letters, 2005, 17(12): 2568-2570.
[16] SOLEHMAINEN K, KAPULAINEN M, HARJANNE M, et al. Adiabatic and multimode interference couplers on silicon-on-insulator [J]. IEEE Photonics Technology Letters, 2006, 18(21): 2287-2289.
[17] SUN D G, LIU Z, ZHA Y, et al. Thermo-optic waveguide digital optical switch using symmetrically coupled gratings [J]. Optics Express, 2005, 13(14): 5463-5471.
[18] SEOK T J, QUACK N, HAN S, et al. Large-scale broadband digital silicon photonic switches with vertical adiabatic couplers [J]. Optica, 2016, 3(1): 64.
[19] SUN D G. A proposal for digital electro-optic switches with free-carrier dispersion effect and Goos-Hanchen shift in silicon-on-insulator waveguide corner mirror [J]. Journal of Applied Physics, 2013, 114(10): 4502.
[20] SUN D G. Manipulation of the coherent spatial and angular shifts of Goos-Hnchen effect to realize the digital optical switch in silicon-on-insulator waveguide corner [J]. Journal of Applied Physics, 2016, 120(18): 333-703.
[21] JOUSHAGHANI A, KRUGER B A, PARADIS S, et al. Sub-volt broadband hybrid plasmonic-vanadium dioxide switches [J]. Applied Physics Letters, 2013, 102(6): 061101.
[22] CHAN C C, TAMIR T. Angular shift of a Gaussian beam reflected near the Brewster angle[J]. Optics Letters. 1985, 10(1): 378-380.
[23] SIMON R, TAMIR T. Nonspecular phenomena in partly coherent beams reflected by multilayered structures[J]. Journal of the Optical Society of America A,1986, 3(4): 558-565.
[24] MüLLER L B, THARANGA D, STAHLHOFEN A, et al. Nonspecular shifts of microwaves in partial reflection[J]. Europhysics Letters, 2006, 73(4), 526-532.
[25] AIELLO A, MERANO M, WOERDMAN J P. Duality between spatial and angular shift in optical reflection[J]. Physical Review A, 2009, 80(6): 061801.
[26] CHU T, YAMADA H, ISHIDA S, et al. Compact 1 × N thermo-optic switches based on silicon photonic wire waveguides [J]. Optics Express, 2005, 13(25): 10109-10114.
[27] DENSMORE A, JANZ S, MA R, et al. Compact and low power thermo-optic switch using folded silicon waveguides [J]. Optics Express, 2009, 17(13): 10457-10465.
[28] SUN P, REANO R M. Submilliwatt thermo-optic switches using free-standing silicon-on-insulator strip waveguides [J]. Optics Express, 2010, 18(8): 8406-8411.
[29] AHARONI H, PLESSIS M D. The spatial distribution of light from silicon LEDs [J]. Sensors and Actuators A: Physical, 1996, 57(3): 233-237.
[30] XU K. Integrated silicon directly modulated light source using p-well in standard CMOS technology [J]. IEEE Sensors Journal, 2016, 16(16): 6184-6191.
[31] KAIKAI X. Silicon MOS optoelectronic micro-nano structure based on reverse-biased PN junction [J]. Physica Status Solidi A, 2019, 216(7): 1800868.